IEEE Robotics and Automation Letters (RAL) paper presented at the
2020 IEEE/RSJ International Conference on Intelligent Robots and Systems (IROS)
October 25-29, 2020, Las Vegas, NV, USA (Virtual)

Flight Path Planning of Solar-powered UAV for Sustainable Communication Relay*

Giancarlo Eder Guerra Padilla[1], Kun-Jung Kim[1], Seok-Hwan Park[2], *Member, IEEE*, and Kee-Ho Yu*[,1], *Senior Member, IEEE*

***Abstract*— Communication is a key aspect of modern life. Unfortunately, when natural disasters occur, the communication system and infrastructure of a city may be partially or even completely destroyed. In this case, communication becomes a crucial part of search-and-rescue missions. This study develops an aerial communication relay platform as an effective solution for communication loss during a natural disaster. The model used considers the aircraft altitude and attitude, which affect the energy acquisition and consumption, and the signal fading effects. The flight path is planned by adopting a nonlinear optimization technique, i.e., the Hermite-Simpson collocation method. For a realistic communication model regarding urban signal loss and path propagation, the building deployment of an area of radius 2km in two cities in South Korea (Seoul and Jeonju) was obtained. Simulation experiments for the different urban environments were performed to test the communication reliability, focusing on the relation between the unmanned aerial vehicle and ground users. Through the simulation, the optimal flight paths in high-rise urban and urban microcell environment were obtained. The obtained results were later compared with a baseline simulation composed of a steady-flight circular path. The generated flight path proves the feasibility of endurance flights for low-altitude communication aid aircrafts using a unified model for signal fading alongside solar power energy acquisition into the case study.**

I. Introduction

Communication systems and devices that enhance the lifestyle and comfort of people have experienced considerable development. Challenges arise during the occurrence of natural disasters causing significant damage to a city. Owing to the possibility of multiple cases of communication loss in the aftermath of natural disasters [1–2], a fast-deployment communication aid platform is vital for search-and-rescue missions [3]. Related developments in the field of unmanned aerial systems for long-endurance aerial communication platforms include high-altitude long- endurance (HALE) designs, such as the solar-powered unmanned aerial vehicle (UAV) Aquila developed by Facebook [4]. The primary goal of the HALE-type UAV design is to loiter around a certain region at heights above 12 km, serving as an atmospheric satellite demonstrated in [5,6]. Besides having a high operational cost, these types of aircrafts have a relative slow deployment response to disaster situations. Conversely, low-altitude long-endurance (LALE) UAVs commonly operate below 5000 m and are inexpensive and rapidly deployable aircrafts, as demonstrated in related studies covering the aircraft conceptual design, energy awareness and wind effects [7–9]. In other studies, flight path planning and power allocation were obtained using a model reduction approach [10] and branch-and-bound approach for unit quaternions [11]. Despite providing good results, they did not provide sufficient proof regarding their flexibility for long-term flight on different type of environments. On the other hand, studies on an aerial communication platform for natural disasters investigated the problem partly. As reported in [12], the outage performance in fading channels was analyzed for a fixed-wing UAV. Moreover, studies such as [13,14] considered channel modeling for aerial platforms primarily without applications in a real-world scenario long-term missions. Thus, this work aims to address the lack of communication systems and countermeasures following natural disasters. To obtain a unified simulation framework, the proposed approach provides a modeling and flight path planning methodology for a sustainable communication platform of a fixed-wing solar-powered UAV under a realistic operational environment based on the information of building composition. The approach introduces the methodology for the deployment of a low-altitude solar-powered UAV communication relay platform over any city by analyzing the energy model, signal propagation, urban signal loss model, and flight path optimization. First, the energy model of the UAV is derived according to the harvested energy and power consumption. Then, the communication model is defined considering the signal path loss and shadowing. The line-of-sight (LOS) & non-line-of-sight (NLOS) probabilities can be calculated by obtaining the building composition data of a certain city. Finally, flight path optimization provides the UAV trajectory seeking a sustainable signal link between the UAV and the ground user (GU) considering the solar energy acquisition and communication constraints.–The rest of the paper is organized as follows. Section II presents the model of the proposed solar-powered UAV, including kinematic and dynamic equations, energy acquisition and consumption, and wireless communication. The preliminary analysis is stated in Section III. The optimization procedure and problem statement are described in Section IV. The simulation conditions, parameters and numerical results are presented in Section V. The discussion and conclusions are given in Sections VI and VII, respectively.

* This work was supported by the National Research Foundation of Korea (NRF-2017R1D1A1B03029381).

[1]G. E. Guerra-Padilla, K.-J. Kim and K.-H. Yu are part of the Aerospace Robotics and Mechatronic Laboratory, Department of Aerospace Engineering, Jeonbuk National University, Jeonju, Republic of Korea (corresponding author: +82-63-270-2471; fax: +82-63-270-2472; e-mail: yu@jbnu.ac.kr).

[2]S.-H. Park is with the Communication Signal Processing Laboratory, Department of Electronic Engineering, Jeonbuk National University, Jeonju, Republic of Korea (e-mail: seokhwan@jbnu.ac.kr).

II. MODELING

A. Solar Radiation

For a solar-powered UAV, one of the key points to consider is the relation between the solar panel surfaces and the sun irradiance rays. Moreover, the solar energy harvesting must be considered a crucial point in the modeling to assure a long term flight for the communication platform application. The solar radiation intensity varies significantly with the relation between the sun and the observer. In this study, an aircraft with zero dihedral angle was considered [15]. Consequently, the angles produced by the sun on the solar cell surface can be derived. First, the declination angle δ is calculated considering the day of the year n (when Jan 1st n=1, Aug 15th n=227), as follows:

$$\delta = 23.45 \sin\left(360 \frac{284+n}{365}\right). \quad (1)$$

Depending on the geographic coordinates (latitude and longitude), the day of the year, and the time of the day, the angles produced by the sun can be calculated as follows:

$$\alpha_s = \sin^{-1}(\cos\phi_{lat} \cos\delta \cos\omega + \sin\delta \sin\phi_{lat}), \quad (2)$$

$$\theta_z = \cos^{-1}(\cos\phi_{lat} \cos\delta \cos\omega + \sin\delta \sin\phi_{lat}), \quad (3)$$

$$\gamma_s = sign(\omega)\left|\cos^{-1}\left(\frac{\sin\delta\cos\phi_{lat} - \cos\omega\cos\delta\sin\phi_{lat}}{\sin\theta_z}\right)\right|, \quad (4)$$

where α_s is the solar altitude angle, θ_z is the zenith angle, γ_s is the solar azimuth angle, ϕ_{lat} is the latitude and ω is the hour angle, which is the angle between the sun at standard-time noon and solar-time noon. The solar azimuth angle calculated in (4) can be positive or negative depending on the hour angle (when $\omega < 0$, the sign is negative; otherwise, positive)[16].

B. UAV Equations of Motion

The UAV model was derived for the calculation of the optimization problem. Fig. 1 shows the coordinate system used to describe the UAV model. To simplify the calculations, the UAV is assumed to fly on a flat, non-rotating earth. Therefore, the point-mass kinematic and dynamic equations considering the UAV motion and aerodynamics can be written as:

$$\begin{aligned} \dot{x} &= V\cos\gamma\cos\psi + W_x, \\ \dot{y} &= V\cos\gamma\sin\psi + W_y, \\ \dot{z} &= V\sin\gamma, \end{aligned} \quad (5)$$

$$\begin{aligned} \dot{V} &= \frac{T - D - mg\sin\gamma}{m} - \dot{W}_x\cos\psi\cos\gamma - \dot{W}_y\sin\psi\cos\gamma, \\ \dot{\gamma} &= \frac{L\cos\phi - mg\cos\gamma}{mV} + \frac{\dot{W}_x\cos\psi\sin\gamma - \dot{W}_y\sin\psi\sin\gamma}{V}, \\ \dot{\psi} &= \frac{L\sin\phi}{mV\cos\gamma} + \frac{\dot{W}_x\sin\psi - \dot{W}_y\cos\psi}{V\cos\gamma}, \end{aligned} \quad (6)$$

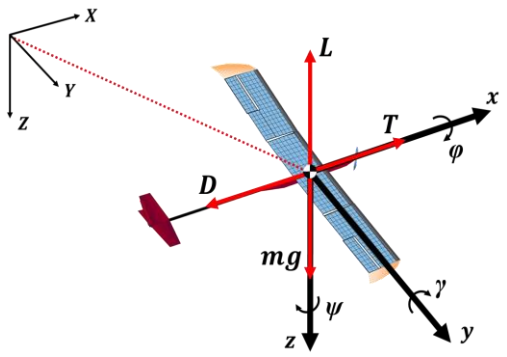

Figure 1. Coordinate frame of solar-powered UAV with the applied forces.

where x is the east position, y is the north position, and z is the altitude. V is the airspeed, ψ is the heading angle, γ is the flight path angle, ϕ is the roll angle, (W_x, W_y) are the wind speeds, $(\dot{W}_x, \dot{W}_y)$ are the wind accelerations, T is the thrust, D is the drag, and L is the lift [17]. The lift and drag can be calculated as:

$$L = 0.5\rho V^2 S C_L, \quad (7)$$

$$D = 0.5\rho V^2 S C_D, \quad (8)$$

where, ρ is the air density, S is the wing area, and C_L, C_D are the lift and drag coefficients, respectively.

C. Communication Model

The analysis of the connectivity between an antenna and a receiver can be approximated with the help of various channel models. To model this relation correctly, the concept of path loss is defined as the signal dispersion caused by the distance between the transmitter and the receiver. The path loss can be evaluated using the following equations:

$$P_{Rx} = P_{Tx} + K - 10\varepsilon\log_{10}\left(d_{TR}/d_0\right), \quad (9)$$

$$K = -20\log_{10}\left(4\pi d_0/\lambda\right), \quad (10)$$

where K represents a unitless constant that depends on the antenna characteristics and is calculated as in (10), P_{Tx} is the antenna transmission power, d_0 is a reference distance for the antenna far-field, λ is the signal wavelength, ε is the path loss exponent, and d_{TR} is the distance from transmitter to the receiver [18,19]. The exponent path loss can be calculated as follows:

$$\varepsilon = a - bh_{Tx} + \frac{c}{h_{Tx}}. \quad (11)$$

TABLE I. PATH LOSS EXPONENT MODEL PARAMETERS

Terrain Category	*a* [-]	*b* [m^{-1}]	*c* [m]
A (Hilly/Moderate-to-Heavy Tree Density)	4.6	0.0075	12.6
B (Hilly/Light Tree Density or Flat/ Moderate-to-Heavy Tree Density)	4.0	0.0065	17.1
C (Flat/Light Tree Density)	3.6	0.0050	20.0

The path loss exponent depends on the environment in which the signal is being transmitted. This value can be approximated using h_{Tx}, which is the altitude of the transmitter, and the numerical data a, b, c in Table I [20,21]. The type B terrain (a=4.0, b=0.0065, c=17.1) is chosen in this study. An urban environment to simulate different types of building deployments can be generated using a statistical model that requires certain parameters describing the built-up areas. The empirical parameters, environment types, and mathematical expressions for the building generation are based on the ITU-R P.1410-5 statistical model [22]. The parameters α_b, β_b, and γ_b indicate the ratio of land area covered by buildings to the total land area, the mean number of buildings per unit area, and a parameter determining the building height distribution, respectively. To represent a realistic model of the city for the simulation, the urban signal loss model is obtained according to the data acquired from the KOSIS (Korean Statistical Information Service) database [23] and the data recollected from the OpenStreetMap® online server [24] as shown in Table II.

To compute the probability of LOS ($P(LOS)$) coverage for the given α_b, β_b and γ_b, we first estimate the number of buildings for a path of length b_r as shown in (12). Then the LOS probability can be obtained as:

$$b_r = floor(r_x \sqrt{\alpha_b \beta_b}), \tag{12}$$

$$P(LOS) = \prod_{i}^{b_r} \left[1 - \exp\left(- \frac{\left[h_{Tx} - \frac{(i+1/2)(h_{Tx} - h_{Rx})}{b_r} \right]^2}{2\gamma_b^2} \right) \right], \tag{13}$$

where r_x (km) is the ground distance between the transmitter and the receiver, h_{Rx} is the ground receiver height, and i is the product index. The P(LOS) follows a Rayleigh distribution [25], and it represents the occurrence probability of a certain group (LOS, NLOS).

In the case of signal fading, we considered the standard path loss with the shadowing occurring when obstacles affect the signal ray. It has been confirmed empirically that the log-normal distribution accurately conveys the variation in path loss in outdoor propagation models [26]. The log-normal distribution can be expressed as follows:

$$p(\varphi_{dB}) = \frac{\xi}{\sqrt{2\pi}\sigma_{\varphi_{dB}}} \exp\left[- \frac{\left(10\log_{10}\varphi_{dB} - \mu_{\varphi_{dB}} \right)^2}{2\sigma_{\varphi_{dB}}^2} \right], \tag{14}$$

TABLE II. STATISTICAL DATA FOR JEONJU AND SEOUL

Environment	*Jeonju (example of urban)*	*Seoul (example of high-rise urban)*
Total area [km^2]	16	16
Number of buildings [-]	8,625	14,414
α_b [-]	0.425	0.650
β_b [buildings/km^2]	539.06	900.88
γ_b [m]	15	30

where, φ_{dB} is the path loss of the shadowing model, $\xi = 1/\ln 10$, $\mu_{\varphi_{dB}}$ is the mean of $\varphi_{dB} = 10\log_{10}\varphi$ in decibels, and $\sigma_{\varphi_{dB}}$ is the standard deviation of φ_{dB} in decibels [27]. The path loss and shadowing impacts are typically imposed to capture the power falloff versus distance along the random attenuation. To find the resulting path loss PL_{total} (dB), it is important to find the path loss and shadowing for LOS and NLOS first, which are expressed as

$$\begin{aligned} PL_{LOS} &= 10\log_{10} K - 10\varepsilon \log_{10}\left(d_{TR}/d_0 \right) + \varphi_{dB} + \zeta_{LOS}, \\ PL_{NLOS} &= 10\log_{10} K - 10\varepsilon \log_{10}\left(d_{TR}/d_0 \right) + \varphi_{dB} + \zeta_{NLOS}. \end{aligned} \tag{15}$$

$$PL_{total} = PL_{LOS} \times P(LOS) + PL_{NLOS} \times P(NLOS), \tag{16}$$

where $\zeta_{LOS}, \zeta_{NLOS}$ are random components in decibels added as a localization variability by utilizing log-normal distribution with zero mean, and $P(NLOS)$ is the probability of having an NLOS, which can also be expressed as $1 - P(LOS)$. The resulting path loss can be expressed in watts through a conversion from decibel units.

After considering the terrain and building distribution in the calculation of the total path loss and shadowing, the signal strength is evaluated by using the received signal strength indicator (*RSSI*) [28] defined as

$$RSSI = P_{Tx} + PL_{total}. \tag{17}$$

D. Energy Model

After calculating the angles produced by the sun over a surface, and the equations that define the UAV motion, the energy harvested and consumed can be expressed. For the energy acquisition, the incidence angle of the sun over the solar cells can be expressed as:

$$\begin{aligned} \theta_i = \cos^{-1}(&\sin\alpha_s \cos\phi \cos\gamma - \cos\alpha_s \sin\phi \sin(\gamma_s - \psi) \\ &+ \cos\alpha_s \cos\phi \sin\gamma \cos(\gamma_s - \psi)). \end{aligned} \tag{18}$$

Therefore, the acquired solar energy can be expressed as:

$$P_{in} = \eta_{cell}\eta_{MPPT} S_{cell} G_i K_t \cos\theta_i, \tag{19}$$

where η_{cell} is the solar cell efficiency, η_{MPPT} is the efficiency of the maximum power point tracker (MPPT), S_{cell} is the solar cell area, G_i is the solar radiation and K_t is the clearness index, which defines the percentage of solar radiation received by the solar cells in different weather conditions. The total output power can be expressed as:

$$P_{out} = \frac{TV}{\eta_{prop}} + P_{av} + P_{Tx}, \tag{20}$$

where P_{av} is the avionics power, η_{prop} is the propeller efficiency, P_{Tx} was defined previously in (9), and T, V are the thrust and velocity, respectively.

The battery state-of-charge (*SOC*) is a relation between the current charge and the maximum charge. The battery power can be defined as the difference between power input and output according to the following rule [29]:

$$P_{bat} = \begin{cases} P_{in} - P_{out} & , SOC < 1 \text{ or } P_{in} - P_{out} < 0 \\ 0 & , SOC = 1 \text{ and } P_{in} - P_{out} > 0 \end{cases}. \quad (21)$$

III. Preliminary Analysis

Before solving the optimization problem, the UAV flight altitude range, and antenna selection were analyzed. For the antenna selection, proper antenna equipment can be selected by considering the altitude range and payload limitations. For the flight altitude range, the aim is to assure a long-term flight while providing a stable signal to the GUs. The values obtained are later included in the flight path optimization. Here, the preliminary studies are described.

A. Antenna Selection and Coverage Area Analysis

The type of antenna should be selected depending on the mission. As the UAV is expected to fly with velocities close to the stall speed, a directional antenna was considered with slight changes in the attitude angles. The antenna is set to be installed in the lower part of the airframe, pointing vertically to the ground. The decisive factors for the selection of the antenna include the antenna weight, power, and beamwidth angles. Hence, the consideration of a moving antenna (tilt in azimuth/elevation) is rejected due to weight restrictions. A panel-type antenna was chosen after a survey of the different types of antennas in the market, and considering the payload weight limitation. Table III shows the specifications of the panel antenna chosen in this study.

With the help of the Antenna Toolbox of MATLAB, the representation of the signal coverage over a city can be obtained through a path propagation simulation [30]. In this study, the building composition is added to the urban signal loss model from the OpenStreetMap database, where the building composition of any city can be retrieved.

To find the appropriate coverage area, multiple simulations were conducted considering the steady-state flight of a UAV with a constant altitude of 400m over an urban environment. Table IV shows the comparative analysis for different coverage areas according to the radius. This preliminary study includes the antenna specifications, the city building composition of an urban environment, and the signal quality of the GUs. Furthermore, the average value of the *RSSI* along with the standard deviation (σ_{RSSI}) is calculated from the five GUs. In conclusion, the data obtained provided an insight into the changes in the remaining energy and *RSSI* values with respect to the coverage area resulting in the selection of an area of radius 2 km for the simulation analysis in the following sections.

TABLE III. Specifications of Antenna Model [31]

Parameter	***Value***
Antenna size [mm]	110×110×75
Antenna weight [kg]	0.300
Antenna power [W]	10
Frequency [GHz]	2.4
Antenna gain [dB]	10
Beamwidth [°]	H50 V50

TABLE IV. Comparative Analysis for Coverage Area

Radius of coverage area [km]	***Remaining energy of battery at sunrise of 2nd day [%]***	***Average RSSI*** (σ_{RSSI}) ***[dBm]***
2	13.88	-63.68 (3.7)
3	15.21	-71.38 (4.0)
4	17.48	-77.09 (4.3)
5	19.07	-81.63 (4.9)
6	21.69	-85.05 (5.3)

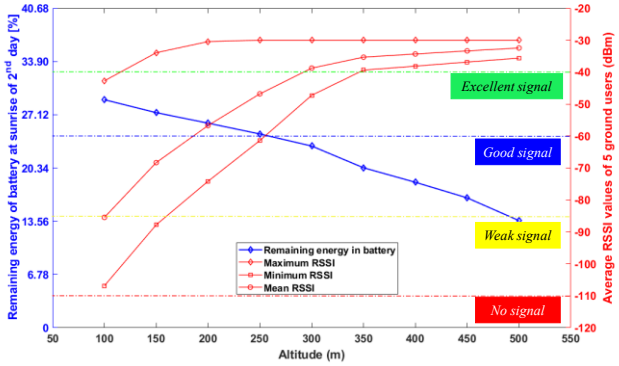

Figure 2. Remaining energy of the battery at the sunrise of the 2nd day and the average *RSSI* values of five GUs for different flight altitudes.

B. Consideration of Flight Altitude Range

The flight altitude range was determined according to a 24-h steady-state flight at different altitudes over a circular trajectory of radius 1.5 km. The operational environment is defined to be an urban area with a type B terrain. The results from the remaining energy of the UAV after the second sunrise, and the average received signal strength over different flight altitudes were obtained. The *RSSI* calculation was performed at different ground points located at the center of every quadrant. The condition is to have a minimum signal quality at which communication is possible and to have sufficient energy remaining in the battery for long-term flight after flying overnight. Fig. 2 shows the results of the trade-off between the remaining energy at the sunrise of the 2nd day, with the *RSSI* average value of five GUs. The maximum, mean and minimum *RSSI* values were evaluated for five GUs located inside the circular coverage area. From this analysis, the range of $[200, 500]m$ corresponds to the altitudes that make the curves of the supplied signal and the remaining energy after the second sunrise of the 2nd day lie inside the admissible trade-off values.

IV. Optimization

A. Methodology

The optimization problem is solved using the Hermite-Simpson direct collocation method [32], which is a nonlinear optimization technique that employs the approximation of the state and control variables with piecewise continuous polynomials. After considering various nonlinear approaches, the direct collocation method was noted to handle complex constraints, and being advantageous in terms of computational time and robustness. The state variables $[\, x, y, z, V, \gamma, \psi, SOC \,]$ and control variables $[\, T, \phi, C_L \,]$ are subject to the aircraft's equations of motion

previously stated in (5) and (6), the battery *SOC* in (21), and the boundary conditions. The mission is considered to fly between the specified initial and terminal values in the time interval $[t_0, t_f]$. At low angles of attack, the lift coefficient (C_L) is considered to be directly proportional to the flight path angle (γ). Constraints are determined to satisfy the UAV's maneuverability and aerodynamic properties, and battery capacity of the UAV. For communication relay operations, flight is limited from 200 m to 500 m as previously deduced from Section III.B. The velocity of the UAV is bounded by its stall speed and its maximum velocity is determined by its aerodynamic characteristics. To generate a smooth flight path, the heading angle rate is limited to satisfy $|\dot{\psi}| \le \dot{\Omega} = 0.1\,[\text{rad/s}]$.

The objective function is set to maximize the remaining energy during flight. Previous experience showed that including the *RSSI* variable in the cost function with a weighted method does not affect the simulation results significantly. Therefore, the *RSSI* level is evaluated for all the GUs as a non-linear constraint, and it should satisfy a minimum admissible value required to maintain a connection between the users and the mobile platform.

$$\max J = \int_{t_0}^{t_f} \left(P_{bat}\right) dt \tag{22}$$

$$\begin{aligned} s.t. \quad & -2km \le x, y \le 2km, \\ & 200m \le h \le 500m, \\ & V_{stall} \le V \le V_{\max},\ 0 \le T \le T_{\max}, \\ & RSSI \ge -110dBm, \\ & 0.1 \le SOC \le 1, \quad Eq.(5-6) \\ & |\gamma| \le 5°, |\phi| \le 10° \\ & |\psi| \le 2\pi, |\dot{\psi}| \le 0.1 rad/s, \\ & -0.087 \le C_L \le 1.081 \end{aligned}$$

The fmincon function included in the OptimTraj [33] MATLAB toolbox is utilized for specifically solving the continuous time trajectory optimization problem. The procedure is shown in Fig. 3 for a better understanding of the optimization methodology. Here, the optimization flow starts with the definition of the expected initial and end points. The initialization is achieved by stating the simulation parameters, grid size, and a guess of the possible final state chosen accordingly from previous attempts in the search of high convergence rate. Then, the system model using the equations derived in Section II is employed. Subsequently, the objective function is analyzed, and the optimization is performed to generate the optimal flight path. The number of iterations is defined empirically from multiple simulation trials, resulting in a division of 96 nodes of 15 minutes each, for the lapse of a 24-h simulation. In this research we used a 6-core (3.7 GHz) processor desktop with Intel i7 CPU and 16GB RAM.

B. Problem Statement

A 24-h simulation was performed for different scenarios to verify the feasibility of the proposed approach. First, the city of Jeonju was chosen to represent an urban environment with a disperse building deployment and relatively low building height. Then, a simulation was performed for the city of Seoul to represent a high-rise urban environment with a higher building density and height. Both these case studies have predetermined GU locations positioned randomly in the map. The path loss and *RSSI* were calculated for six ground points with known position considered to be the GUs. Furthermore, the UAV-GU link considered the statistical data from Table II for the *RSSI* calculation. The following assumptions were made to obtain values that converge properly:

- The UAV flight is performed in an environment where the wind influence is considered constant in the northeast direction (x-axis as north, and y-axis as east) with wind components ($W_x = 2\,m/s$, $W_y = 1\,m/s$).
- A multipath signal is assumed to not affect the transmitted signal ray so that the effect of destructive and constructive signal rays is neglected.
- The solar-powered UAV flight speed along the trajectory is estimated to be close to the stall speed; hence, the Doppler effect caused by the moving transmitter can be neglected.

The UAV specifications and boundary constraints were obtained from the calculations stated in the previous section. Table V presents the specifications assigned to the UAV model for the simulation.

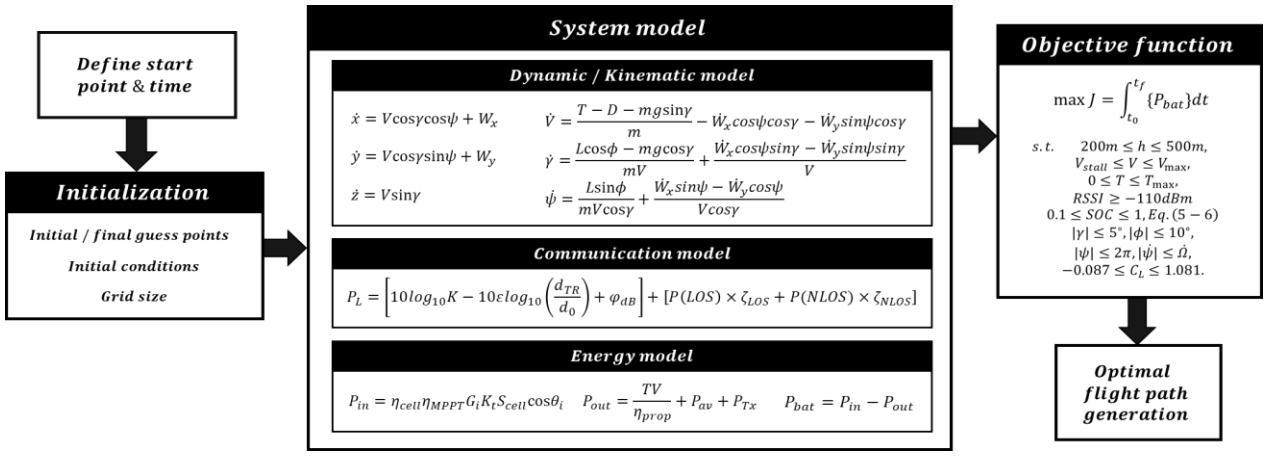

Figure 3. Path planning procedure for optimal flight trajectory.

TABLE V. SPECIFICATIONS OF THE UAV MODEL [34]

Parameter	*Value*	*Parameter*	*Value*
m_{UAV} [kg]	3.152	$m_{payload}$ [kg]	0.400
AR [-]	13	S [m^2]	0.837
S_{cell} [m^2]	0.645	η_{cell} [-]	0.225
η_{MPPT} [-]	0.95	η_{prop} [-]	0.65
$SoC_{\max}$ [Wh]	294	P_{av} [W]	3.9

TABLE VI. SIMULATION CONDITIONS

Parameter	*Value*
Simulation date	2019.08.13 06:00am
Weather condition	Clear sky ($K_t = 1$)
Simulation duration [hr]	24
Initial battery *SOC* [%]	50
Initial position (lat, long) [º]	Jeonju UAV-Tx [35.8123, 127.1204] Seoul UAV-Tx [37.5726, 126.9874]

Table VI shows the simulation conditions. The simulation is set to start at 06:00 a.m. local time, in the cities of Jeonju and Seoul, in South Korea. The initial battery charge is set at 50% and the starting position is at the origin (0,0) at an altitude of 400m. The GUs are positioned randomly inside the area. The geographical coordinates were converted to Cartesian coordinates using the Universal Transverse Mercator (UTM) coordinate system by setting the initial point [E 330187.91, N 3964765.78] as (0,0).

V. SIMULATION

Two different scenarios are studied in this section. One corresponds to the city of Jeonju, South Korea, which has an urban environment with a relatively low-altitude low-density building composition. The other case corresponds to the city of Seoul, South Korea, which consists of a high-rise urban environment with a higher building density and average building height. Fig. 4 shows the simulation results obtained from the optimized and non-optimized (circular flight path with constant altitude) approaches for an urban environment. In the figures, the optimized and non-optimized simulation results are shown in blue-red and green colors, respectively. Fig. 4(a) shows the coverage map for the operational environment, which is an urban environment in this case, such as the city of Jeonju. Fig. 4(b) shows the optimal flight path, which is subdivided into blue color for daytime flight, and red color for nighttime flight. The baseline case is shown in green color, reflecting a constant altitude circular flight path. The flight path obtained from the optimization shows the UAV flying inside the range of the GUs, constantly changing its attitude to acquire the maximum energy possible from the sun. After sunset, the UAV performs a glide descend reducing the thrust control [35]. During nighttime, the flight path of the UAV shows a tendency to navigate toward the center of the area. Fig. 4(c) presents the comparison between the baseline and optimal *RSSI* values for each GU located randomly inside the coverage area. The comparison of the results from the optimal approach with the baseline results shows an increase along the UAV trajectory. Fig. 5 shows the results obtained from the optimization compared with those from a non-optimized simulation for a sector in the city of Seoul. The intricate path generated by the optimization can be

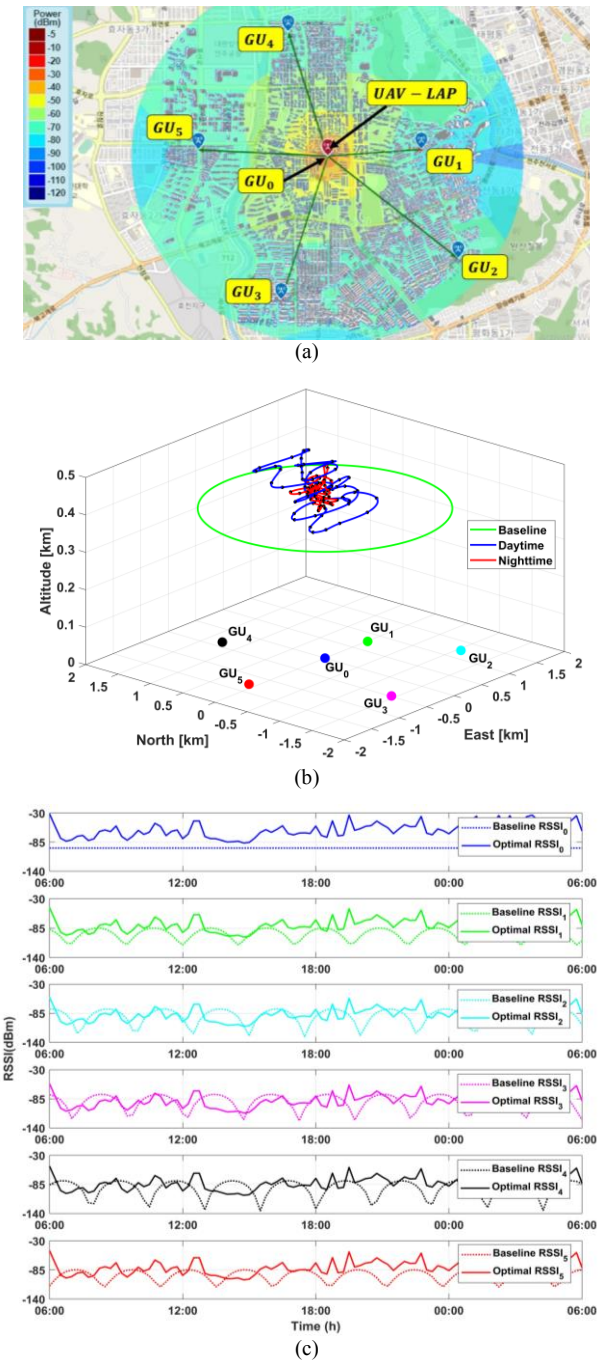

Figure 4. Simulation results for an urban environment (Jeonju, South Korea): a) Signal coverage map over the operational environment; b) UAV flight path for the baseline and optimized cases; c) *RSSI* level for each GU.

understood as the UAV seeking the maximum energy acquisition while satisfying the constraints, specifically the *RSSI* constraint. Fig. 5(a) shows the coverage map over the operational environment for a high-rise urban environment such as the city of Seoul. Fig. 5(b) shows the optimal flight path for the high-rise urban environment. Comparing with the urban environment case, it shows a narrower flight path caused by the presence of high buildings. Fig. 5(c) represents the comparison between the baseline and optimal *RSSI* values at each GU located randomly in the city of Seoul.

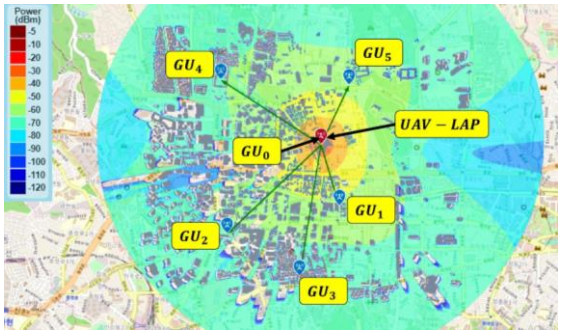

(a)

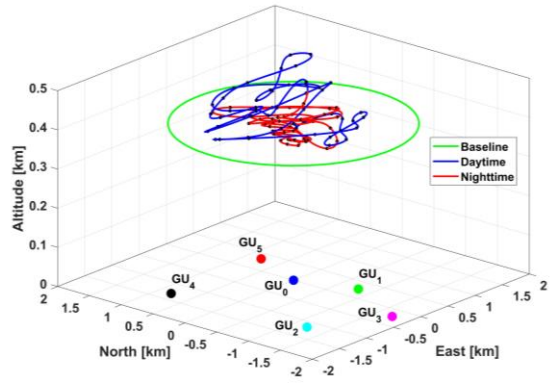

(b)

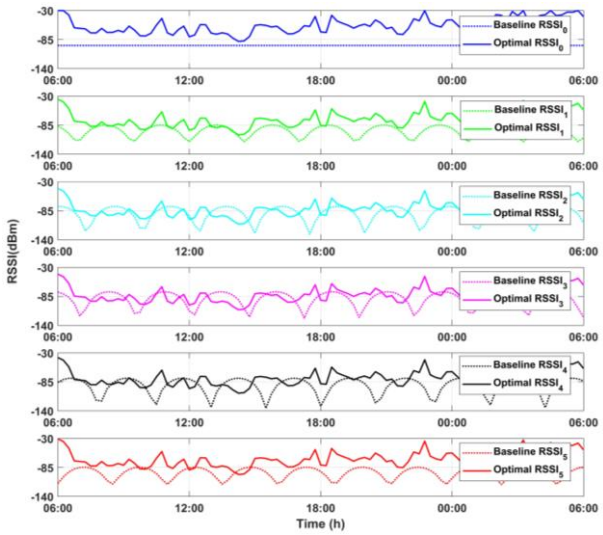

(c)

Figure 5. Simulation results for a high-rise urban environment (Seoul, South Korea): a) Signal coverage map over the operational environment (Central district of Seoul); b) UAV flight path for the baseline and optimized approaches; c) *RSSI* level for each GU.

To provide a real-world application example, the optimization problem was performed under different values of clearness index as shwon in Fig. 6. The results of a simulation case for the city of Seoul using our approach were as follows: for clear sky conditions ($K_t = 1$) the *SOC* at the second sunrise is 27.75%, for cloudy skies ($K_t = 0.5$) the *SOC* is 5.26%, and for overcast weather ($K_t = 0.1$), the *SOC* is -33.10%. For the overcast example, the battery was drained within a few hours after midnight ($P_{bat} = 0$ at 01:48am), and the energy deficit prevented the UAV from staying airborne until the next day.

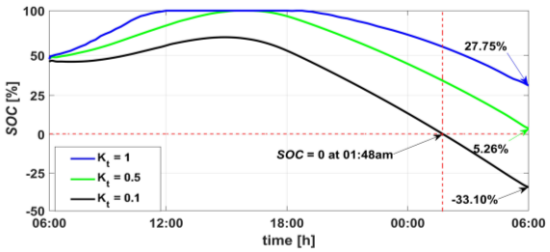

Figure 6. Remaining battery *SOC* percentage after the sunrise of the 2nd day depending on different clearness index (K_t) values.

VI. Discussion

This study focuses on the relation between the signals relayed by the UAV and the GUs. The link between the UAV and the ground control station (GCS) was not considered. Notably, this paper presents only the numerical simulation results. Furthermore, the OpenStreetMap server has a limitation on the number of extractable features, only allowing a limited area selection. In this study, the GUs are assumed to be static points. Furthermore, point-to-point *RSSI* calculation was not considered due to a high complexity and large computational time present when including the building characteristics. The results for the flight path over the cities of Jeonju and Seoul show the UAV loitering in an area close to the static GUs. The UAV follows a controlled descent, performing a glide maneuver after the sunset. The nighttime flight path loiters around the center point because the power input value is zero, and the optimization only seeks to minimize the power consumption. This causes the flight path of the UAV to narrow into the center point. When comparing the average *RSSI* levels between the urban and high-rise urban environments, the results for the high-rise urban case are lower, showing that the presence of high altitude buildings affects the average *RSSI* values. The signal strength is varied according to the UAV position change with respect to the GUs, and it lies inside the range of connectivity. The computational times of the simulations are: 1872.3 s and 1911.1 s for the optimal cases (Jeonju and Seoul, respectively), and 115.2 s for the baseline simulations. After the sunrise of the 2nd day, the battery *SOC* of the optimal case compared with that of the baseline (13.78%) showed a percentage point increase of 20.35 and 13.97, for Jeonju and Seoul, respectively. The battery *SOC* results obtained are appropriate, because the minimum *SOC* value allowed for long-term flight is considered to be over 20%. In the case of the battery *SOC* with respect to the clearness index, the amount of harvested solar energy varied considerably after the sunrise of the 2nd day. Furthermore, for an overcast type weather, failure to achieve long-term flight due to battery draining at 01:48am was observed. Although, constant wind field was considered in this study, real wind field data will be utilized in future studies. Moreover, solar radiation prediction using machine-learning algorithms to estimate the energy available under different weather conditions will be studied. Moving GUs and multi-UAV formations can also be applied for coverage area increase. In this matter, point-to-point *RSSI* calculation will also be studied. Furthermore, the inclusion of no-fly zones such as airports, government facilities, and military bases can be considered for the flight path planning.

VII. CONCLUSIONS

In this paper, a 24-h simulation for the flight path planning of a communication relay platform, considering the parameters of an urban environment for signal loss modeling was reported. An appropriate propagation model was selected to express the changes in the signal received. The path loss model highlighted the effects of the signal loss on the distance to the signal wave, and the shadowing fading channel provided the wave diffraction and scattering effects from obstacles. Moreover, the urban signal loss depending on the environment building deployment was considered. The results obtained from the optimal flight path simulation showed an improvement in signal quality with respect to the non-optimized case. This approach also allows the UAV to fly overnight while maintaining a stable link between the UAV and the GUs. Therefore, the communication sustainability of a solar-powered UAV platform over urban environments was verified. The use of continuous-flight aerial platforms for disaster relief aids and communication appears to be a promising area of study.

REFERENCES

[1] H. Yamamura et al., "Communication Problems After the Great East Japan Earthquake," *Disaster Med public Health Prep.*, vol. 8, issue 4, 2014, pp. 293–296.

[2] E. Chapin et al., "Impact of the 2007 Ica Earthquake on Health Facilities and Health Service provision in Southern Peru" *Prehospital and Disaster Medicine*, vol. 24, issue 4, 2009, pp. 326–332.

[3] J. Delmerico et al., "Active Autonomous Aerial Exploration for Ground Robot Path Planning," *IEEE Robotics and Automation Letters*, vol. 2, issue 2, 2017, pp. 664–671.

[4] D. Coldewey, (2018, June 26) "Facebook permanently grounds its Aquila solar-powered internet plane," retrieved from https://techcrunch.com/2018/06/26/facebook-permanently-grounds-its aquila-solar-powered-internet-plane.

[5] N. J. Colella and G. S. Wenneker, "Pathfinder. Developing a solar rechargeable aircraft," *IEEE Potentials*, 1996, pp. 18─23.

[6] G. Weiss, "Around the World In a Solar Plane," *IEEE Spectrum*, vol. 41, 2004, pp. 12─14.

[7] P. Oettershagen et al., "Design of small hand-launched solar-powered UAVS: From concept study to a multi-day world endurance record flight," *Journal of Field Robotics*, vol. 34, 2017, pp. 1352─1377.

[8] D. H. Choi et al., "Energy-aware path planning of an unmanned aerial vehicle acting as a communication relay for mobile ground nodes," *Proceedings of the Institution of Mechanical Engineers, Part G: Journal of Aerospace Engineering*, vol. 233, no. 3, 2018, pp. 1124-1132.

[9] W. H. Al-Sabban et al., "Wind-energy based path planning for Unmanned Aerial Vehicles using Markov Decision Processes," *2013 IEEE International Conference of Robotics and Automation*, 2013, pp. 784–789.

[10] S. Hosseini, R. Dai, and M. Mesbani, "Optimal Path Planning and Power Allocation for Long Endurance Solar-powered UAV," *2013 American Control Conference,* Washington DC, USA, 2013.

[11] R. Dai et al., "Optimal Path Planning for Solar-powered UAVs based on Unit Quaternions," *2012 IEEE 51st Conference on Decision and Control (CDC),* Maui, USA, 2012.

[12] P. Oettershagen et al., "Meteorology-Aware Multi-Goal path Planning for Large-Scale Inspection Missions with Long-Endurance Solar-Powered Aircraft," *Journal of Aerospace Information Systems*, vol. 16 no. 10, 2017, pp. 390-408.

[13] X. Jiang et al., "Outage Probability Optimization for UAV-enabled Wireless Relay Networks in Fading Channels," *Physical Communication*, vol. 33, 2019. pp. 35─45.

[14] A. Al-Hourani et al., "Modeling Air-to-Ground Path loss for Low Altitude Platforms in Urban Environments," *2014 IEEE Global Communications Conference*, 2014, pp. 2898─2904.

[15] J.-S. Lee, H.-B Park, and K.-H. Yu, "Flight Path Optimization of Solar Powered UAV for Endurance Flight," *SICE Annual Conference*, 2015, pp. 820–823.

[16] J. A. Duffie, and Beckman, W. A., *Solar Engineering of Thermal Processes*, 3rd ed. Wiley, Hoboken, New Jersey, 2006.

[17] J. D. Anderson, *Aircraft performance and design*, vol. 1, McGraw-Hill, New York, 2006, pp. 238.

[18] A. Goldsmith, *Wireless Communications*, vol. 1, Cambridge University Press, 2006.

[19] T. S. Rappaport, *Wireless Communications – Principle and Practice*, 2nd edition, Prentice Hall, 2001.

[20] A. Al-Hourani et al., "Modeling Cellular-to-UAV Path-loss for Suburban Environments," *IEEE Wireless Communications Letters*, vol. 7, no. 1, 2018, pp. 82–85.

[21] V. Erceg, et al., "An empirically based path loss model for wireless channels in urban environments," *IEEE Journal on Selected Areas in Communications*, 1999, pp. 1205–1211.

[22] "*Propagation data and prediction methods required for the design of terrestrial broadband radio access systems operating in a frequency range from 3 to 60 GHz*," Recommendation ITU-R P.1410-5, 2012.

[23] Korean Statistical Information Service. (2020). Construction/Housing/Land Info 2018. [Data file]. Retrieved from http://kosis.kr/eng/statisticsList/statisticsListIndex.do?menuId=M_01_01&vwcd=MT_ETITLE&parmTabId=M_01_01

[24] OpenStreetMap® (2020). Building composition of the city of Jeonju and Seoul. [Data file]. Retrieved from https://www.openstreetmap.org/export#map=13/35.8301/127.1286&layers=H.

[25] M. K. Simon, and M.-S. Alouini, *Digital Communication over Fading Channels*, Wiley, New York, 2000.

[26] J. Holis and P. Pechac, "Elevation Dependent Shadowing Model for Mobile Communications via High Altitude Platforms in Built-Up Areas," *IEEE Transactions on Antennas and Propagation*, vol. 56, no.4, 2008, pp. 1078–1084.

[27] N. Kostov, "Mobile Radio Channels Modeling in MATLAB," *Society for Radioelectronic Engineering,* 2003, vol. 12, pp 12–16.

[28] J. Xu et al., "Distance Measurement Model Based on RSSI in WSN," *Wireless Sensor Networks*, vol. 2, no. 8, Aug. 2010, pp. 606–611.

[29] S. H. Kim, G. E. Guerra-Padilla, K. J. Kim, and K. H. Yu, "Flight Path Planning for a Solar Powered UAV in Wind Fields Using Direct Collocation," *IEEE Transactions on Aerospace and Electronic Systems*, vol. 56, no. 2, 2020, pp. 1094–1105.

[30] G. E. Guerra-Padilla, K. J. Kim, and K. H. Yu, "Communication Relay Applications of a Solar-powered UAV Following a Collision-free Optimal Flight Path," *APISAT 2019 Asia Pacific International Symposium on Aerospace Technology*, Gold Coast, Australia, 2019.

[31] LawMate 2.4GHz 10dBi Panel Antenna for Wireless Video Transmission & Long Range FPV (2020). Retrieved from https://dronesvision.net/lawmate-2-4ghz-10dbi-panel-antenna-for-wireless-video-transmission-long-range-fpv/.

[32] B. Geiger., "Unmanned aerial vehicle trajectory planning with direct methods," Ph.D. dissertation, The Pennsylvania State University, 2009.

[33] M. Kelly, (2017). Transcription Methods for Trajectory Optimization: a beginners tutorial, retrieved from arXiv:1707.00284v1.

[34] H. B. Park, "Virtual Flight Experiment and Performance Evaluation of Solar Powered UAV," M.S Thesis, Chonbuk National University, Department of Aerospace Engineering, 2016.

[35] J.-S. Lee, and K.-H. Yu, "Optimal Path Planning of Solar-Powered UAV Using Gravitational Potential Energy," *IEEE Transactions on Aerospace and Electronic Systems*, vol. 53, no.3, 2017, pp. 1442–1451.